Results in Output-Trajectory Redesign for Flexible Structures," *Journal of Dynamic Systems, Measurement, and Control*, Vol. 120, No. 4, 1998, pp. 456–461.

[5]Yim, W., and Singh, S. N., "Nonlinear Inverse and Predictive End Point Trajectory Control of Flexible Macro-Micro Manipulators," *Journal of Dynamic Systems, Measurement, and Control*, Vol. 119, No. 3, 1997, pp. 412–420.

[6]Snell, S. A., Enns, D. F., and Garrad, W. L., Jr., "Nonlinear Inversion Flight Control for a Supermaneuverable Aircraft," *Journal of Guidance, Control, and Dynamics*, Vol. 15, No. 4, 1992, pp. 976–984.

[7]Zou, Q., and Devasia, S., "Preview-Based Stable-Inversion for Output Tracking," *Journal of Dynamic Systems, Measurement, and Control*, Vol. 121, No. 4, 1999, pp. 625–630.

[8]Gupta, N. K., "Frequency Based Cost Functions: Extensions to Linear-Quadratic-Gaussian Design Methods," *Journal of Guidance and Control*, Vol. 3, No. 6, 1980, pp. 529–535.

[9]Ortega, J. M., *Matrix Theory: A Second Course*, Plenum, New York, 1987, pp. 151–154.

[10]Zhou, K., Doyle, J. C., and Glover, K., *Robust and Optimal Control*. Prentice–Hall, Upper Saddle River, NJ, 1996, pp. 104–110.

[11]Brinkerhoff, R., "Output Tracking in Actuator Deficient/Redundant Systems: Theoretical and Experimental Results," M.S. Thesis, Mechanical Engineering Dept., Univ. of Utah, Salt Lake City, UT, Dec. 1999.

Flight Control Design of an Automatic Landing Flight Experiment Vehicle

Atsushi Fujimori* and Munerou Kurozumi†
Shizuoka University,
3-5-1 Johoku, Hamamatsu 432-8561, Japan
and
Peter N. Nikiforuk‡ and Madan M. Gupta§
University of Saskatchewan,
Saskatoon, Saskatchewan S7N 5A9, Canada

I. Introduction

THE National Aerospace Laboratory (NAL) and the National Aerospace Development Agency (NASDA) in Japan have been developing an unmanned reentry space vehicle, named HOPE-X, for a decade.[1] An Automatic Landing Flight Experiment vehicle called ALFLEX, which is a 37%-sized model of the HOPE-X, has been studied to develop an automatic landing control system. To implement a reliable automatic control system on the HOPE-X, several control design techniques have been proposed.[2–5] Sunazawa and Ohta[3] used the inverse dynamics transformation to compensate the nonlinearity of the ALFLEX. Miyajima and Kuze[4] applied neural networks to navigate the ALFLEX a reference trajectory. The NAL/NASDA designed a guidance and control law using multiple delay models and a multiple design points method.[5]

This Note presents an alternative flight control design of the ALFLEX using a fuzzy gain-scheduling (FGS) state-feedback technique in the frame of a double-loop control system (DLCS). The DLCS consists of the inner and the outer loops that are used for stabilizing the controlled system and tracking the command, respectively. In this Note, an inner-loop controller is designed by the FGS state-feedback technique[6] to guarantee the stability over the entire operating range of the ALFLEX, whereas the outer-loop controller is designed so as to improve the tracking property. The proposed control design method is applied to a numerical simulation program for an automatic landing test of the ALFLEX[2] to evaluate control performance of the designed control law.

Received 30 March 1999; presented as Paper 99-4057 at the AIAA Guidance, Navigation, and Control Conference, Portland, OR, 9–11 August 1999; revision received 7 October 1999; accepted for publication 7 October 1999.

*Associate Professor, Department of Mechanical Engineering; a-fujimori@eng.shizuoka.ac.jp.
†Graduate Student, Department of Mechanical Engineering.
‡Dean Emeritus, Department of Mechanical Engineering.
§Professor, Department of Mechanical Engineering.

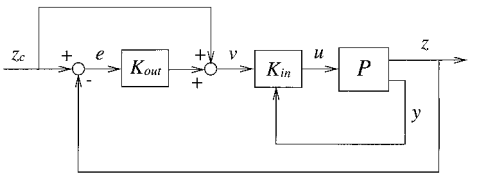

Fig. 1 Double loop control system.

II. Double-Loop Control System

Figure 1 shows a block diagram of a DLCS applying to the ALFLEX. z is the controlled variable, z_c is its command input, y is the feedback variable, u is the control input, and v is the inner-loop command input. P is a controlled plant, K_{in} is an inner-loop controller, and K_{out} is an outer-loop controller. The ALFLEX is an unstable controlled plant, and contains nonlinear factors and uncertainties. The control system for the ALFLEX therefore, should be designed not only to stabilize, but also to compensate for tracking error $e \triangleq z_c - z$ due to the nonlinear factors and uncertainties. Then, the inner loop is used for augmenting the stability of the system, whereas the outer loop is used for reinforcing the tracking property.

Now, let us discuss the outer loop of Fig. 1 using linear transfer functions. Let T_{zv} be a transfer function from v to z. A transfer function from z_c to z, T_{zz_c} is then written as

$$T_{zz_c} = (I + T_{zv}K_{\text{out}})^{-1}T_{zv}(I + K_{\text{out}}) \tag{1}$$

If K_{in} is designed so as to stabilize the controlled plant and satisfy $T_{zv}(0) = I$, the steady-state of z for a step command z_c is given by

$$z(\infty) = \lim_{s \to 0} sT_{zz_c}(s)(1/s)z_c = z_c \tag{2}$$

The servo condition, $z(\infty) = z_c$, is always satisfied. Then, K_{out} is designed so as to stabilize T_{zv} and improve the tracking property of T_{zz_c}.

III. Inner-Loop Design Using FGS State-Feedback

This section describes a design of the inner-loop controller using a FGS state-feedback technique.[6] A controlled plant considered in this study is given by the following nonlinear system:

$$\dot{x}(t) = f[x(t), u(t)], \qquad z(t) = g[x(t), u(t)] \tag{3}$$

where $u(t)$, $z(t)$, and $x(t)$ are m-dimensional input, p-dimensional controlled variable, and n-dimensional state vectors, respectively. It is assumed that $x(t)$ is available for feedback; that is, $y(t) = x(t)$ in Fig. 1.

Over the operating range of the system, let us select r linearized points (x_i^d, u_i^d) $(i = 1, \ldots, r)$ and construct a linear time-invariant (LTI) model for each linearized point. Let η_j $(j = 1, \ldots, g)$ be variables that recognize the linearized points, and N_{ji} $(i = 1, \ldots, r)$ be fuzzy sets of η_j. Fuzzy rules representing a nonlinear system [Eq. (3)] is given as follows:

If $\eta_1 = N_{1i}$ and $\cdots$ and $\eta_g = N_{gi}$, then the nonlinear system Eq. (3) is approximated by

$$\begin{bmatrix} \dot{x}(t) \\ z(t) \end{bmatrix} = \begin{bmatrix} A_i & B_i \\ C_i & D_i \end{bmatrix} \begin{bmatrix} x(t) - x_i^d \\ u(t) - u_i^d \end{bmatrix} + \begin{bmatrix} 0 \\ z^d \end{bmatrix}, \qquad (i = 1, \ldots, r) \tag{4}$$

where

$$A_i \triangleq \frac{\partial f(x_i^d, u_i^d)}{\partial x^T}, \qquad B_i \triangleq \frac{\partial f(x_i^d, u_i^d)}{\partial u^T}$$

$$C_i \triangleq \frac{\partial g(x_i^d, u_i^d)}{\partial x^T}, \qquad D_i \triangleq \frac{\partial g(x_i^d, u_i^d)}{\partial u^T}$$

N_{ji} is characterized by the membership function $\mu_{ji}(\eta_j)$. To evaluate the suitability of a given set of η_j $(j = 1, \ldots, g)$, the degree of satisfaction $h_i(\eta)$ is given as

$$h_i(\eta) \triangleq \mu_{1i}(\eta_1) \wedge \cdots \wedge \mu_{gi}(\eta_g), \qquad (i = 1, \ldots, r) \tag{5}$$

where $\eta \triangleq [\eta_1 \cdots \eta_g]^T$. $\wedge$ is the minimum operator in fuzzy logic. That is, the larger $h_i(\eta)$ is, the more suitable the ith LTI model [Eq. (4)] for the nonlinear system [Eq. (3)] is. Moreover, let $\alpha_i(\eta)$ be defined as the normalized degree of satisfaction

$$\alpha_i(\eta) \triangleq \frac{h_i(\eta)}{\sum_{i=1}^{r} h_i(\eta)}, \qquad (i = 1, \ldots, r) \tag{6}$$

where

$$\alpha_i(\eta) \geq 0, \qquad \sum_{i=1}^{r} \alpha_i(\eta) = 1 \tag{7}$$

Then, a model which corresponds to the entire operating range, that is, a defuzzified model, is given by

$$\begin{bmatrix} \dot{x}(t) \\ z(t) \end{bmatrix} = \sum_{i=1}^{r} \alpha_i(\eta) \left\{ \begin{bmatrix} A_i & B_i \\ C_i & D_i \end{bmatrix} \begin{bmatrix} x(t) - x_i^d \\ u(t) - u_i^d \end{bmatrix} + \begin{bmatrix} 0 \\ z_i^d \end{bmatrix} \right\} \tag{8}$$

It is called the fuzzy model of the nonlinear system [Eq. (3)]. The fuzzy rule of state-feedback laws is given as follows: If $\eta_1 = N_{1i}$ and $\cdots$ and $\eta_g = N_{gi}$, Then a state-feedback law is given by

$$u(t) = -F_i\left[x(t) - x_i^d\right] + u_i^d + v(\eta), \qquad (i = 1, \ldots, r) \tag{9}$$

where F_i $(i = 1, \ldots, r)$ are $m \times n$ feedback gains. Equation (9) gives state-feedback laws for r-linearized points. Similar to the fuzzy model, a state-feedback law that corresponds to the entire operating range is given by

$$u(t) = -\sum_{i=1}^{r} \alpha_i(\eta)\left\{ F_i\left[x(t) - x_i^d\right] - u_i^d \right\} + v(\eta) \tag{10}$$

Equation (10) is called the FGS state-feedback. Substituting Eq. (10) into Eq. (8), the closed inner-loop system is written as

$$\begin{bmatrix} \dot{x}(t) \\ z(t) \end{bmatrix} = \begin{bmatrix} \tilde{A}_F(\eta) & \tilde{B}(\eta) \\ \tilde{C}_F(\eta) & \tilde{D}(\eta) \end{bmatrix} \begin{bmatrix} x(t) \\ v(\eta) \end{bmatrix} + \begin{bmatrix} w_1^d(\eta) \\ w_2^d(\eta) + \tilde{z}^d(\eta) \end{bmatrix} \tag{11}$$

where

$$\tilde{A}_F(\eta) \triangleq \sum_{i=1}^{r}\sum_{j=1}^{r} \alpha_i(\eta)\alpha_j(\eta)(A_i - B_i F_j)$$

$$\tilde{B}(\eta) \triangleq \sum_{i=1}^{r} \alpha_i(\eta) B_i$$

$$\tilde{C}_F(\eta) \triangleq \sum_{i=1}^{r}\sum_{j=1}^{r} \alpha_i(\eta)\alpha_j(\eta)(C_i - D_i F_j)$$

$$\tilde{D}(\eta) \triangleq \sum_{i=1}^{r} \alpha_i(\eta) D_i$$

$$w_1^d(\eta) \triangleq \sum_{i=1}^{r}\sum_{j=1}^{r} \alpha_i(\eta)\alpha_j(\eta)\left\{ B_i(F_j x_j^d + u_j^d) - (A_i x_i^d + B_i u_i^d) \right\}$$

$$w_2^d(\eta) \triangleq \sum_{i=1}^{r}\sum_{j=1}^{r} \alpha_i(\eta)\alpha_j(\eta)\left\{ D_i(F_j x_j^d + u_j^d) - (C_i x_i^d + D_i u_i^d) \right\}$$

$$\tilde{z}^d(\eta) \triangleq \sum_{i=1}^{r} \alpha_i(\eta) z_i^d$$

The feedback gains F_i $(i = 1, \ldots, r)$ are designed to guarantee the global stability over the entire operating range with the Lyapunov function. On the other hand, $v(\eta)$ is designed to regulate $z(t)$ to an a priori specified values.

The closed-loop system [Eq. (11)] without external signals, that is, $\dot{x}(t) = \tilde{A}_F(\eta)x(t)$, is quadratically stable only if there exists a positive-definite function $V(t) \triangleq x^T(t)X^{-1}x(t)$ such that

$$\dot{V}(t) \leq -x^T(t)\left(Q + \sum_{i=1}^{r} \alpha_i(\eta) F_i^T R_i F_i \right) x(t) \tag{12}$$

where

$$Q \geq 0, \qquad R_i > 0, \qquad (i = 1, \ldots, r)$$

Since the external signals in Eq. (11), $w_1^d(\eta)$, $w_2^d(\eta)$, $\tilde{z}^d(\eta)$, and $v(\eta)$, are bounded, the above stability condition is also held for Eq. (11) with the external signals. Feedback gains F_i $(i = 1, \ldots, r)$ which satisfy the above quadratic stability condition are parameterized by linear matrix inequalities (LMIs) in the following theorem.[6]

Theorem 1. Equation (12) is held only if there exists a positive-definite-matrix X and matrices M_i $(i = 1, \ldots, r)$ such that

$$\begin{bmatrix} A_i X + X A_i^T - B_i M_i - M_i^T B_i^T & XH^T & M_i^T \\ HX & -I_p & 0 \\ M_i & 0 & -R_i^{-1} \end{bmatrix} \leq 0 \tag{13}$$

$$(i = 1, \ldots, r)$$

$$\begin{bmatrix} (A_i + A_j)X + X(A_i + A_j)^T - (B_i M_j + B_j M_i) - (B_i M_j + B_j M_i)^T & XH^T \\ HX & -\frac{1}{2} I_p \end{bmatrix} \leq 0$$

$$(i = 1, \ldots, r,\ j = i + 1, \ldots, r) \tag{14}$$

where $Q = H^T H$ and rank $Q = p$. Then, F_i $(i = 1, \ldots, r)$ in Eq. (10) are given by

$$F_i = M_i X^{-1}, \qquad (i = 1, \ldots, r) \tag{15}$$

□

From Eq. (11), the steady-states of $x(t)$ and $z(t)$ are obtained as

$$x(\infty) = -\tilde{A}_F^{-1}\left[w_1^d + \tilde{B} v(\eta) \right] \tag{16}$$

$$z(\infty) = \tilde{C}_F x(\infty) + \tilde{D} v(\eta) + w_2^d + \tilde{z}^d \tag{17}$$

Therefore, the inner-loop command input $v(\eta)$ which the controlled variable is settled to $z(\infty) = z_c$ is given by

$$v(\eta) = (\tilde{D} - \tilde{C}_F \tilde{A}_F^{-1} \tilde{B})^{-1}(z_c - \tilde{z}^d + \tilde{C}_F \tilde{A}_F^{-1} w_1^d - w_2^d) \tag{18}$$

IV. Numerical Simulation of ALFLEX Flight Control

A. Design of DLCS

This section presents a numerical simulation in which the proposed control design method was applied to the ALFLEX flight control problem. In the automatic landing flight test, the ALFLEX was dropped from a helicopter at the altitude of 1500 m with the initial velocity of 46 m/s (Ref. 2). Since the ALFLEX had no thrusting equipment, the trajectory of the ALFLEX was monotonously descendent. In this Note, a reference trajectory was given in terms of the reference flight velocity V_{air}^* and the reference flight path angle Γ^* with respect to the altitude H. Then, the variable η for constructing the fuzzy model was given by

$$\eta = \eta_1 = H \tag{19}$$

The nonlinear ALFLEX model [Eq. (3)] was linearized at the six equilibrium points as shown in Table 1. The equilibrium condition was that the dynamic pressure and the flight path angle were constant. At each equilibrium point, a linearized equation of the ALFLEX was separated into the longitudinal and the lateral LTI equations. Membership function of H, μ_H, is shown in Fig. 2. Using the degree of satisfaction

$$\mu_H(H) = h_1(H) = \alpha_1(H) \tag{20}$$

fuzzy models were constructed for the longitudinal and the lateral directions, respectively.

Matlab and LMI Control Toolbox[7] were used to find a positive-definite-matrix X and matrices M_i $(i = 1, \ldots, 6)$, satisfying Eqs. (13) and (14), and obtain the state-feedback gains F_i $(i = 1, \ldots, 6)$ in Eq. (15). The inner-loop transfer function T_{zv} at $H = 600$ m was used to design K_{out}. In this simulation, K_{out} whose order was four was obtained by the linear quadratic Gaussian technique to stabilize T_{zv} and to improve the tracking property of T_{zz_c}.

B. Simulation Results

The designed DLCS was evaluated by a simulation program for an automatic landing flight test of the ALFLEX. The program included several components of the ALFLEX: aerodynamic models, actuators, atmospheric condition, measurement systems, etc.[2] A simulation of the single-loop control system (SLCS) in which the outer loop was removed from the designed DLCS was also done for comparison.

Table 1 Linearized points with respect to flight velocity and flight path angle

Parameter	Model 1	Model 2	Model 3	Model 4	Model 5	Model 6
H (m)	1500	1000	600	100	30	1
V_{air} (m/s)	80	80	80	80	60	55
Γ (deg)	−30	−30	−30	−20	−15	−13

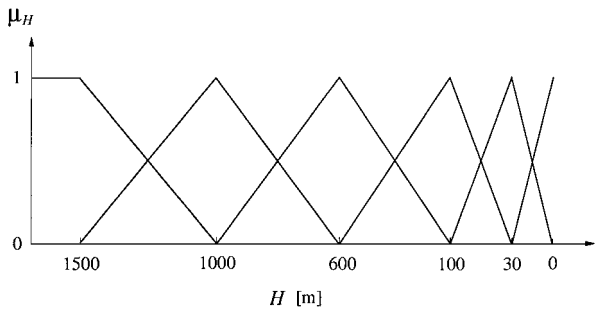

Fig. 2 Membership function of H.

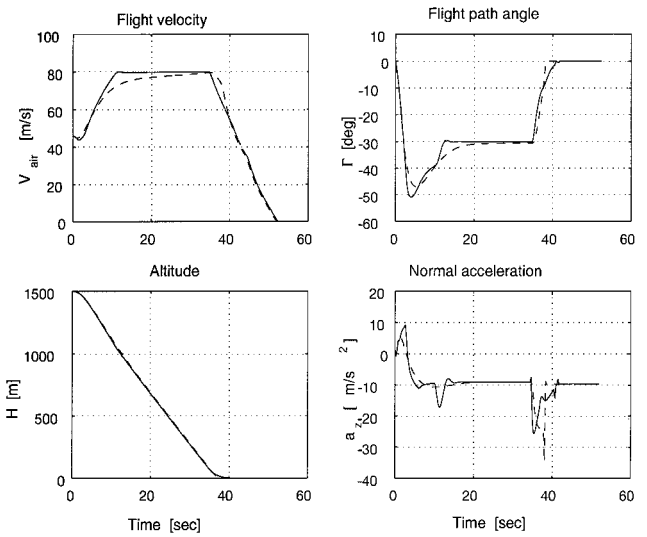

Fig. 3 Time responses of controlled variables from release to landing using DLCS (——) and SLCS (– – –).

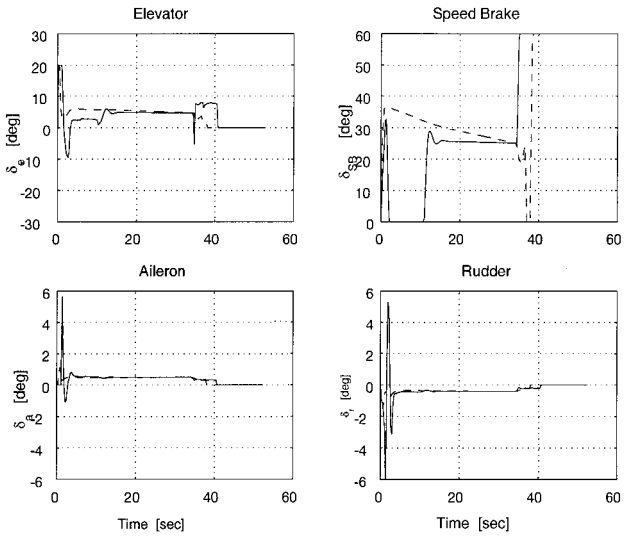

Fig. 4 Time responses of control surfaces using DLCS (——) and SLCS (– – –).

Figures 3 and 4 show the time responses of the controlled variables and the control surfaces, respectively. The solid lines mean the responses using the DLCS, whereas the dashed lines mean the responses using the SLCS. The reference flight velocity and the reference flight path angle for $H > 100$ m were given as $V_{\text{air}}^* = 80$ m/s and $\Gamma^* = -30$ deg. The tracking property of the DLCS was better than that of the SLCS. This result came from the activity of the elevator and the speed brake during the first 10 s as shown in Fig. 4. The outer-loop controller K_{out} provided a complementary input to reduce the tracking errors of V_{air} and Γ. Moreover, the magnitude of the normal acceleration a_z of the DLCS was less than that of the SLCS. Thus, it was seen that the DLCS was useful in improving the tracking performance under the nonlinearity and uncertainties in the controlled plant.

V. Conclusion

This Note has presented a flight control design called ALFLEX using the FGS state-feedback technique in the frame of the DLCS. The inner-loop control law was designed by the FGS state-feedback technique to guarantee the stability over the entire operating range of the ALFLEX, whereas the outer-loop control law was designed so as to improve the tracking property. Applying the proposed control design method to a numerical simulation program for an automatic landing flight test of the ALFLEX, the designed DLCS showed better tracking performance than the SLCS in which the outer loop was removed from the DLCS.

This Note has considered the longitudinal trajectory for landing the ALFLEX. For practical implementation, the lateral trajectory should be taken into account. Furthermore, the position control for landing on a runway is also required. The presented DLCS is applicable for these control objectives of the ALFLEX.

Reference

[1] Davis, N. W., "NASDA Pins Its Hopes on HOPE," *Aerospace America*, Vol. 29, No. 8, 1991, pp. 32–35.

[2] NAL/NASDA ALFLEX Group, "Flight Simulation Model for Automatic Landing Flight Experiment. Part I: Free Flight and Ground Run Basic Model," TR of National Aerospace Lab., Oct. 1994.

[3] Sunazawa, S., and Ohta, H., "Nonlinear Flight Control for a Reentry Vehicle Using Inverse Dynamics Transformation," *Journal of the Japan Society of Aeronautical and Space Sciences*, Vol. 45, No. 516, 1997, pp. 52–61.

[4] Miyajima, K., and Kuze, C., "Application of the Neural Network System to the Longitudinal Control System of the ALFLEX," *Proceedings of the ALFLEX/HOPE Symposium*, Tokyo, 1996, pp. 115–118.

[5] Miyazawa, Y., Ishikawa, K., and Fuji, K., "Guidance and Control Law for Automatic Landing Flight Experiment of Reentry Space Vehicle," *Guidance, Navigation and Control Conference*, Monterey, CA, 1993, pp. 1057–1066.

[6]Fujimori, A., Wu, Z.-Y., Nikiforuk, P. N., and Gupta, M. M., "A Design of a Flight Control System Using Fuzzy Gain-Scheduling," *GNC Conference*, New Orleans, LA, 1997, pp. 1647–1653.

[7]Gahinet, P., Nemirovski, A., Laub, A. J., and Chilali, M., *LMI Control Toolbox*, The Math Works Inc., Natick, MA, May 1995.

Exoatmospheric Interceptor Pulse Motor Optimization with Discrete Bias Removal

Craig A. Phillips* and D. Stephen Malyevac†
U.S. Naval Surface Warfare Center, Dahlgren, Virginia 22448

Nomenclature

t	= time, s
t_g	= time-to-go to the intercept, s
t_{gmc}	= time-to-go to the intercept at the midcourse stage motor burnout (second pulse), s
$t_{\text{gmc min}}$	= minimum allowable time-to-go to the intercept at the midcourse stage motor burnout (second pulse), s
t_{mission}	= the total flight time to the intercept, s
t_{p1bo}	= flight time at burnout of first pulse, s
t_{rm}	= flight time at which the track bias is removed, s
t_2	= burn time of the second pulse, s
V_{MR1}	= average speed remaining to the intercept after midcourse stage first pulse burnout, m/s
ZEM_{BIAS}	= total zero effort miss value at current time due to the target track bias, m
ZEM_{31}	= total zero effort miss value at midcourse stage first pulse burnout, m
ZEM^*	= zero effort miss value at midcourse stage first pulse burnout due to all sources other than the track bias, m
ΔV_{2PUL}	= divert velocity of second pulse allowed for lateral maneuver, m/s
σ^2_{HE}	= variance of the total interceptor attitude navigation and control error, rad^2
σ^2_{VTGT}	= variance of the target velocity measurement error, $(\text{m/s})^2$

Introduction

In this Note, the problem of selecting the pulse split for a two-pulse motor of the exoatmospheric midcourse stage of a notional antitactical ballistic missile interceptor is considered. The pulse split reflects the fraction of total impulse allocated to each pulse. The midcourse stage operates outside the atmosphere during the long period between the separation of the final endoatmospheric stage and the separation of the kinetic kill vehicle (KKV), which contains a seeker and divert system for final homing. Reference 1 demonstrated the use of the mission chart approach for the analysis of these interceptors. This Note extends the methodology of Ref. 1 to include a large bias in the target track. A large bias in the track is defined as one that is greater than the ability of the KKV to correct. A bias in the target track process could be introduced by the following: 1) tracking and engaging the only visible object in the target complex that is not the desired target, 2) tracking all objects in a target complex but being unable to discriminate the desired target, or 3) attempting to engage an undetected object by estimating its states from other information. The bias in the target track is composed of both a position and a velocity component relative to the current true target kinematics. These two components of the error can be combined by extrapolating the velocity bias error through the time-to-go to intercept.

After the desired target and its state estimates are determined, the bias in the target track becomes apparent and the associated heading error is removed by diverting during the next propulsion burn.

Four scenarios are possible for removal of the bias in the target track. The underlying philosophy to these definitions is that for a successful intercept each pulse must be able to remove all of the zero effort miss (3σ value) present at its ignition. The first scenario is defined by the removal of the bias during the first or second pulse burn. Because of the short burn times relative to the mission times, only a relatively small portion of the intercept population will fall under this category, and therefore this scenario is deemed inappropriate for consideration in the pulse split optimization. The second scenario is defined by the removal of the bias before the ignition of the first pulse. This scenario can affect mission timelines but is not a driver in the pulse split optimization. The third scenario is defined by the removal of the bias after the second pulse burn. In this situation, the zero effort miss from the bias in the target track must be removed entirely by the KKV divert. For large biases in the target track greater than the KKV divert, such a mission is infeasible. Modification of the pulse split provides no benefit in this scenario and shall not be pursued. The fourth scenario is defined by the removal of the bias in the target track between the burnout of the first pulse and the ignition of the second pulse. One of the primary uses of a two-pulse motor is to delay the ignition of the second pulse until after the bias in the target track is removed. This last scenario is of greatest operational interest and has the greatest impact on the optimization of the pulse motor.

The remainder of the Note will concentrate on the optimization of the pulse motor for this fourth scenario. The changes to the second pulse timeline constraints when a large bias in the target track is introduced in this scenario are presented. The impact of the pulse split on the requirements placed on the weapon system timeline for removal of the bias in the target track will be demonstrated. Finally, the relationship of the maximum and minimum feasible mission times to the pulse split is discussed for this scenario.

Second Pulse Timeline Constraints in the Presence of a Bias

Reference 1 defined five constraints on the second pulse ignition and burnout timeline. When the bias in the target track is removed between the two pulses, only the minimum time-to-go at the second pulse burnout constraint changes relative to the definition in Ref. 1. The bias in the target track must be included in the errors at first pulse burnout that the second pulse must remove. The errors at second pulse burnout are not affected by the bias in the target track because the scenario defines them as removed by the second pulse.

The magnitude of the bias is considered fixed for this analysis, but its spatial orientation could vary considerably. A conservative approach is used in that the zero effort miss (ZEM) from the bias in the target track is "stacked" with the ZEM from the nominal error tree by assuming they are aligned. Although not strictly correct, it adds another degree of conservatism to the analysis. In this approach, the ZEM at first pulse burnout is given by

$$3\sigma\text{ZEM}_{31} = 3\sigma\text{ZEM}^* + \text{ZEM}_{\text{BIAS}} \tag{1}$$

For a successful intercept, the second pulse must be able to remove all of the zero effort miss (3σ value) present at the first pulse burnout. This requirement determines the minimum allowable time-to-go from second pulse burnout to the intercept. The minimum time-to-go expressed by

$$t_{\text{gmc min}} \approx \frac{3\left(\sigma^2_{\text{HE}} V^2_{\text{MR1}} + \sigma^2_{\text{VTGT}}\right)^{\frac{1}{2}}(t_{\text{mission}} - t_{\text{p1bo}}) + \text{ZEM}_{\text{BIAS}}}{\Delta V_{\text{2PUL}}} \tag{2}$$

Received 1 April 1999; revision received 24 August 1999; accepted for publication 25 August 1999. This material is declared a work of the U.S. Government and is not subject to copyright protection in the United States.

*Lead Functional Design Engineer, Missile Systems Engineering Branch, Weapons Systems Department, Dahlgren Division, G23, 17320 Dahlgren Road. Senior Member AIAA.

†Lead Functional Design Engineer, Missile Systems Engineering Branch, Weapons Systems Department, Dahlgren Division, G23, 17320 Dahlgren Road. Member AIAA.